J Fluoresc (2014) 24:431–444
DOI 10.1007/s10895-013-1309-4

ORIGINAL PAPER

Excited Charge Transfer States in Donor–Acceptor Fluorescent Phenanthroimidazole Derivatives

J. Jayabharathi · V. Thanikachalam · R. Sathishkumar

Received: 19 July 2013 / Accepted: 27 September 2013 / Published online: 20 October 2013

Abstract Solvent-dependent electronic structure of the selected donor (D) acceptor (A) derivatives of phenanthroimidazole derivatives containing fluoro substituent as an electron acceptor fragment in the fluorescent charge transfer (CT) states has been investigated. The mechanism of the radiative charge recombination CT→S_0 is discussed in terms of the Mulliken–Murrell model of the CT complexes and the Marcus theory of photoinduced electron transfer (ET). Solvatochromic effects on the spectral position and profile of the stationary fluorescence spectra clearly indicate the CT character of the emitting singlet states of all of the compounds studied both in a polar and a non polar environment. An analysis of the CT fluorescence leads to the quantities relevant for the electron transfer in the Marcus inverted region. The values of the fluorescence rate constants (k_r) and corresponding transition dipole moments (M) and their solvent polarity dependence indicate that the electronic coupling between the emitting ^{1}CT state and the ground state is a governing factor of the radiative transitions. The relatively large values of M indicate a nonorthogonal geometry of the donor and acceptor subunits in the fluorescent states. It is shown that Marcus theory can be applied for the quantitative description of the radiationless charge recombination processes in the cases when an intersystem crossing to the excited triplet states can be neglected.

Keywords Phenanthroimidazole · Charge transfer · Donor · Acceptor · Lifetime

J. Jayabharathi (✉) · V. Thanikachalam · R. Sathishkumar
Department of Chemistry, Annamalai University,
Annamalainagar 608 002, Tamilnadu, India
e-mail: jtchalam2005@yahoo.co.in

Introduction

The wide investigations of the intramolecular electron transfer (ET) in donor (D)-acceptor (A) compounds such as carbazol-9-yl derivatives of aromatic nitriles [1] and aryl or hetero aryl derivatives of aromatic amines [2] suggest a possibility to predict the photophysical behaviour of a particular D–A molecule from the properties of the individual chromophores as far as the electronic interactions between the lowest excited charge transfer state CT and the ground state S_0 (V_0) and/or the locally excited states LE, localized either in the acceptor ($V_{1,3}{}^A$) or in the donor ($V_{1,3}{}^D$) respectively, are taken into account. A similar approach can be applied to describe the properties of the singlet CT states e.g., the transition dipole moments for the CT absorption (^{1}CT←S_0) and the fluorescence (^{1}CT→S_0) as well as the characteristics of the triplet ^{3}CT states [3] (e.g., the zero-field splitting parameters).

The study of the intramolecular ET reactions is to identify structural elements that promote electronic coupling between an electron donor and an acceptor is a challenging one. The application of different models [4–6] used to determine the electronic matrix elements from the solvent polarity effects on the electronic transition dipole moments of the CT emission (M_{flu}) [7, 8] and the CT absorption (M_{abs}) [2]. The appropriate values of the electronic coupling elements are mainly determined by the interactions between the atoms forming the bond A–D can be theoretically predicted following the formalism proposed by Dogonadze et al. [9, 10]. Neglecting contributions from the σ orbitals, one can obtain for π-electronic systems

$$V_0 = C^A_{\mathrm{LUMO}} C^d_{\mathrm{HOMO}} \beta_{\mathrm{AD}} \cos(\theta_{\mathrm{A--D}}) + \mathrm{const.}, \quad (1)$$

$$V^A_{1,3} = C^{\mathrm{A}}_{\mathrm{HOMO}} C^{\mathrm{D}}_{\mathrm{HOMO}} \beta_{\mathrm{AD}} \cos(\theta_{\mathrm{A--D}}) + \mathrm{const.}, \quad (2)$$

$$V^D_{1,3} = C^{\mathrm{A}}_{\mathrm{LUMO}} C^D_{\mathrm{LUMO}} \beta_{\mathrm{AD}} \cos(\theta_{\mathrm{A--D}}) + \mathrm{const.}, \quad (3)$$

where $\theta_{A\text{-}D}$ denotes the angle between the planes of the acceptor and donor subunits and C_{HOMO} and C_{LUMO} are the LCAO coefficients (as obtained for the individual chromophores) of the $2p_Z$ atomic orbitals (where z is the axis perpendicular to the acceptor or donor rings) of the highest occupied molecular orbital (HOMO) and of the lowest unoccupied molecular orbital (LUMO) located on the atoms forming the A–D bond. β is the resonance integral for these AD atoms and const. is related to the electronic interactions between the remaining pairs of atoms in the D–A molecule (this contribution is usually small and negligible) . Expressions 2 and 3 assume that the ^{1}LE state is mainly described by a configuration corresponding to the HOMO→LUMO excitation (e.g., ^1L_a state in Platt's notation)

In this work, we used the Lippert solvent parameter (Δf), the normalized E_T (30) polarity scale, and the multi parameter Kamlet-Taft and Catalan solvent scales to describe the solvent effect on the fluorescence emission and stokes shift of phenanthroimidazole derivatives. We have also addressed the influence of solvents on the photophysical properties of the synthesized molecules in terms of $hc\tilde{\upsilon}^{vac}_{abs}$, $hc\tilde{\upsilon}^{vac}_{flu}$ and $\left(hc\tilde{\upsilon}^{vac}_{abs}-hc\tilde{\upsilon}^{vac}_{flu}\right)$ with solvent polarity function. The reported results are based on a study of the solvent effects on the spectral position of absorption and fluorescence spectra as well as on the CT emission quantum yields and excited state depopulation kinetics.

Experimental

Chemicals

4-fluorobenzaldehyde and Phenanthrene 9, 10-dione have been supplied by Sigma Aldrich (St. Louis, USA). Aniline, 4-Methylaniline, 4-Methoxyaniline, and 3,5- Dimethylaniline used were of analytical grade and received from S.D. Fine (Mumbai, India).

One Pot Synthesis of Phenanthrimidazoles

Phenanthrimidazole derivatives have been prepared by four components condensation of phenanthrene-9, 10-dione (40 mmol), ammonium acetate (30 mmol), 4-fluorobenzaldehyde (30 mmol) and aniline (30 mmol) refluxed in ethanol at 80 °C in the presence of Indium (III) fluoride (InF_3) as Lewis acid catalyst (Scheme 1) for 30 min. The completion of the reaction was monitored by thin layer chromatography. The reaction mixture was extracted with dichloromethane and purified by column chromatography using benzene: ethyl acetate (9:1) as the eluent.

2-(4-fluorophenyl)-1-phenyl-1H-phenanthro [9,10-d] imidazole (1)

Yield: 94 %. Anal. Calcd. for $C_{27}H_{17}FN_2$: C, 83.49; H, 4.41; N, 7.21. Found: C, 83.61; H, 4.32; N, 7.30. ^{1}H NMR (400 MHz, d6-DMSO): δ 7.07 (d, J=8 Hz, 1H), 7.23 (t, J=7.2 Hz, 2H), 7.36 (t, J=7.2 Hz, 1H), 7.55 (t, J= 8 Hz, 1H), 7.59–7.63 (m, 2H), 7.67–7.72 (m, 6H), 7.78 (t, J=6.8 Hz 1H), 8.69 (d, J=6.8 Hz 1H), 8.88 (d, J=8.4 Hz 1H), 8.93 (d, J=8 Hz 1H). ^{13}C NMR (100 MHz, d6-DMSO): δ 115.16, 115.37, 120.11, 121.96, 122.41, 123.65, 124.48, 125.22, 125.74, 126.63, 126.75, 126.78, 127.46, 127.64, 127.70, 128.47, 129.11, 130.26, 130.35, 131.34, 131.43, 136.34, 137.99, 149.69, 161.08, 163.54. MS: m/z. 389.27 [M^+].

2-(4-fluorophenyl)-1-p-tolyl-1H-phenanthro [9,10-d] imidazole (2)

Yield: 92 %. Anal. calcd. for $C_{28}H_{19}FN_2$: C, 83.56; H, 4.76; N, 6.96. Found: C, 83.95; H, 4.65; N, 7.01. ^{1}H NMR (400 MHz, $CDCl_3$): δ 2.48(s, 3H), 7.13 (d, J= 7.6 Hz, 1H), 7.21 (t, J=8.8 Hz, 2H), 7.35 (t, J=7.6 Hz, 1H), 7.46–7.48 (m, 2H), 7.53–7.63 (m, 5H), 7.68 (t, J= 6.8 Hz 1H), 7.77 (t, J=7.2 Hz, 1H), 8.68 (d, J=8.8 Hz, 1H), 8.87 (d, J=8 Hz, 1H), 8.92 (d, J=8.4 Hz, 1H). ^{13}C NMR (100 MHz, d6-DMSO): δ 20.92, 115.16, 115.37, 120.13, 121.95, 122.48, 123.64, 124.44, 125.19, 125.71, 126.64, 126.82, 126.85, 127.43, 127.62, 127.73, 128.43, 128.77, 13.80, 131.33, 131.41, 135.36, 136.29, 139.79, 149.79, 161.06, 163.52. MS: m/z. 403.44 [M^+].

2-(4-fluorophenyl)-1-(4-methoxyphenyl)-1H-phenanthro [9,10-d] imidazole (3)

Yield: 95 %. Anal. calcd. for $C_{28}H_{19}FN_2O$: C, 80.37; H, 4.58; N, 6.69. Found: C, 81.01; H, 4.25; N, 6.60. ^{1}H NMR (400 MHz, d6-DMSO): δ 3.89 (s, 3H), 7.15–7.25 (m, 5H), 7.38 (t, J=8 Hz, 1H), 7.595–7.67 (m, 6H), 7.76 (t, J=7.6Hz, 1H), 8.66 (d, J=12 Hz, 1H), 8.89 (dd, J= 12 Hz, 2H). ^{13}C NMR (100 MHz, d6-DMSO): δ 60.86, 120.36, 120.65, 125.45, 127.21, 128.85, 129.66, 130.42, 130.92, 131.91, 131.99, 132.20, 132.64, 132.93, 133.18, 133.75, 135.46, 135.72, 136.56, 136.68, 141.55, 155.27, 165.34. MS: m/z. 419.39 [M^+].

2-(4-fluorophenyl)-1-(3,5-dimethylphenyl)-1H-phenanthro [9,10-d] imidazole (4)

Yield: 97 %. Anal. calcd. for $C_{29}H_{21}FN_2$: C, 83.63; H, 5.08; N, 6.73. Found: C, 83.21; H, 5.24; N, 6.38. ^{1}H NMR (400 MHz, d6-DMSO): δ 2.41 (s, 6H), 7.07 (t, J= 8Hz, 2H), 7.15–7.31 (m, 5H), 7.54 (t, J=7.6 Hz, 1H), 7.60–7.68 (m, 3H), 7.73 (t, J=8 Hz 1H), 8.74 (d, J= 7.6 Hz 2H), 8.80 (d, J=8 Hz 1H). ^{13}C NMR (100 MHz, d6-DMSO): δ 20.79, 114.75, 114.96, 120.43, 122.00, 122.35, 122.88, 123.64, 124.76, 125.32, 125.83, 126.20, 126.44, 126.91, 127.54, 127.57, 128.37, 130.83, 130.91, 131.36, 136.19, 137.50, 139.72, 149.26, 161.06. MS: m/z. 417.02 [M^+].

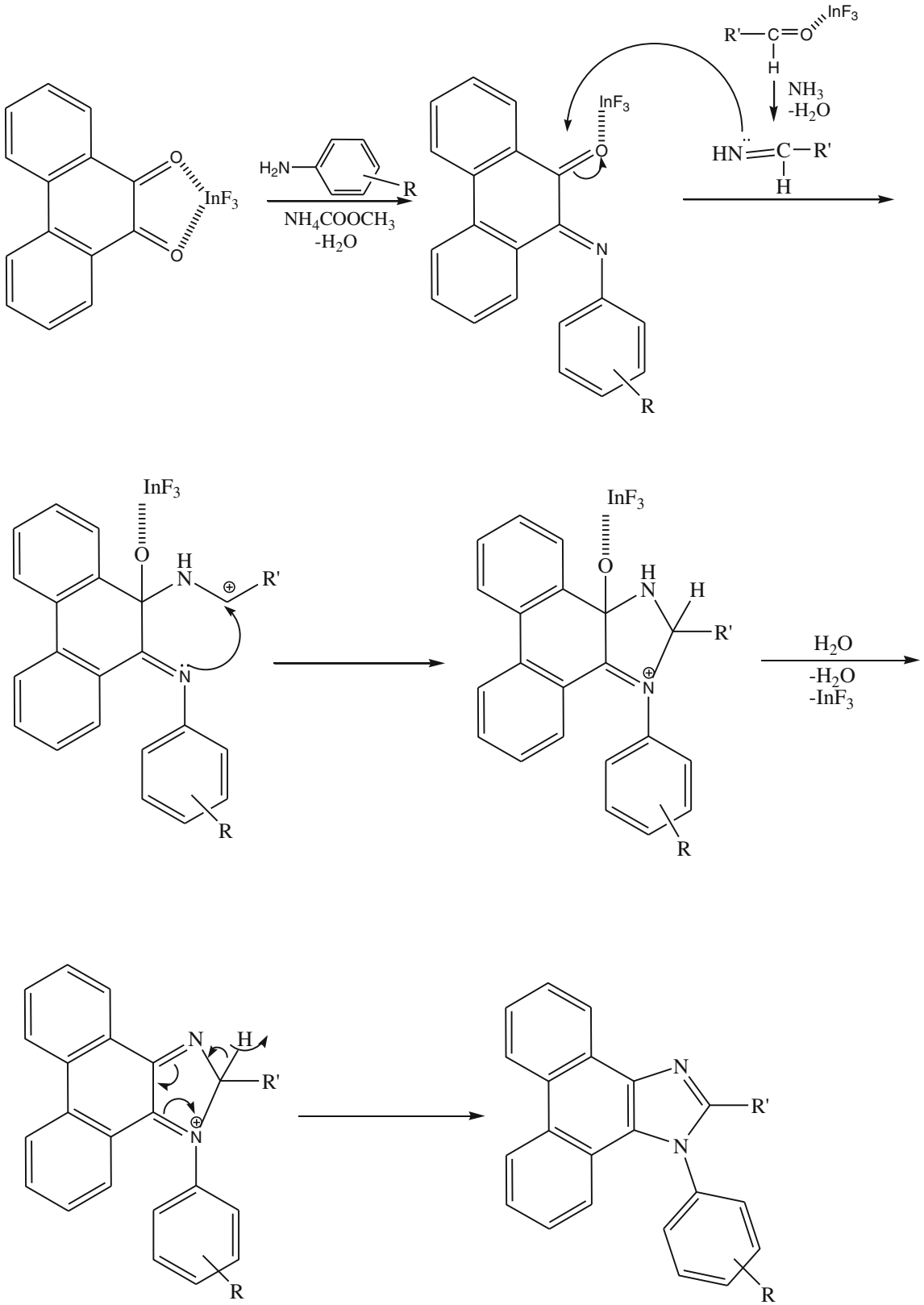

Scheme 1 Possible mechanism of catalytic synthesis of phenanthroimidazole

Spectral Measurements

The infrared spectra have been recorded with an Avatar 330-Thermo Nicolet Fourier transform infrared spectrometer (Thermo, America). The proton spectra at 400 MHz were obtained at room temperature using a Bruker 400 MHz NMR spectrometer (Bruker biospin, California, USA). Proton decoupled ^{13}C NMR spectra were also recorded at room temperature employing a Bruker 400 MHz NMR spectrometer operating at 100 MHz. The mass spectra of the samples were obtained using a Thermo Fischer LC-Mass spectrometer in fast atom bombardment (FAB) mode (Thermo, France). Fluorescence lifetime measurements were carried out with a nanosecond time correlated single photon counting (TCSPC) spectrometer Horiba Fluorocube-01-NL lifetime system with NanoLED (pulsed diode exCitation source) as the excitation source and TBX-PS as detector. The slit width was 8 nm and the laser excitation wavelength was 270 nm. The fluorescence decay was analyzed using DAS6 software.

Table 1 Effect of amount and catalytic activity of catalyst in the synthesis of phenanthroimidazoles (1–4)

S. No	Compound	Time (minutes)	Catalyst (mol %)	Yield
1	1	> 400	No entry	Trace
2	1	30	10	65
3	1	60	10	79
4	1	60	15	94
5	2	> 400	No entry	Trace
6	2	30	10	61
7	2	60	10	74
8	2	60	15	92
9	3	> 400	No entry	Trace
10	3	30	10	63
11	3	60	10	76
12	3	60	15	95
13	4	> 400	No entry	Trace
14	4	30	10	69
15	4	60	10	77
16	4	60	15	97

Result and Discussion

Effect of the Catalytic Activity of Indium (III) Fluoride

Initially, we have carried out the condensation reaction of phenanthrene-9, 10-dione, *p*-fluorobenzaldehyde with substituted anilines in ethanol for 24 h with stirring, in the absence of catalyst and observed only trace amount of products. In order to improve the yield and shorten the reaction time, we have carried out the reaction using different amounts of the catalysts at different time intervals (Table 1). It was observed that the amount of catalyst plays a significant role in controlling the activity of the catalyst. Among the various amounts of catalyst used, 15 mol% was found to be the best in ethanol medium. A possible mechanism is that the reaction proceeds as shown in Scheme 1. The present catalyst is novel and efficient. The salient features of this protocol are high product yields, shorter reaction time, low catalyst loading and easy work-up procedure, which make this procedure quite simple, more convenient and environmentally benign. Hopefully, our methodology could be a valid contribution to the existing processes in the field of phenanthroimidazole synthesis.

Solvent Modulated Absorption and Emission Behaviour

Room temperature absorption and the fluorescence maxima of phenanthroimidazole derivatives (1–4) are shown in Figs. 1 and 2 respectively. The spectra show a superposition of the bands corresponding to the donor and acceptor subunits which seem to be only slightly perturbed by their interactions. The two absorption bands have been assigned to the $^1(\pi–\pi^*)$ states correspond in Platt's notation to the ^1L_b and ^1L_a excited states. The low and high energy transitions, $^1L_b \leftarrow S_0$ and $^1L_a \leftarrow S_0$ respectively, with a relatively high probability can be clearly observed in the absorption spectra of all the compounds studied [11–13]. Detailed inspection of the low-energy absorption region of the D-A phenanthroimidazole derivatives containing fluoro substituents as an electron acceptor clearly indicates the presence of additional charge transfer singlet states. A long wave shoulder attributed to the $^1CT \leftarrow S_0$ transition is also observed. The magnitude of the shifts suggests that the ground state of the molecule is polar.

The emission spectra of 1–4 displayed in Fig. 2, show a red-shifted band in the region of 380–417 nm from hexane to water. The fluorescence maximum is greatly affected by solvent polarity where a red-shifted fluorescence is observed on increasing the solvent polarity. The effect of polarity of the medium on the fluorescence maximum is more intense than that on the absorption maximum. This observation suggests that the emitting state is more polar than the ground state [14–16]. The emission yields are more prominent in polar solvents compared to that of non-polar solvents. The linear variation of the Stokes shift with E_T (30) has been shown in Fig. 3a, where a double linear correlation is obtained [17]. Polar protic solvents fall on a separate line indicating that the mode of solvation of the emitting state is different from that in the other polar aprotic solvents. For polar protic solvents, gradual increment of Stokes shift is due to intermolecular hydrogen bonding interactions. The studied compounds exhibit overall increase of Stokes shift from non-polar to polar aprotic solvents mainly due to combined effect of increasing

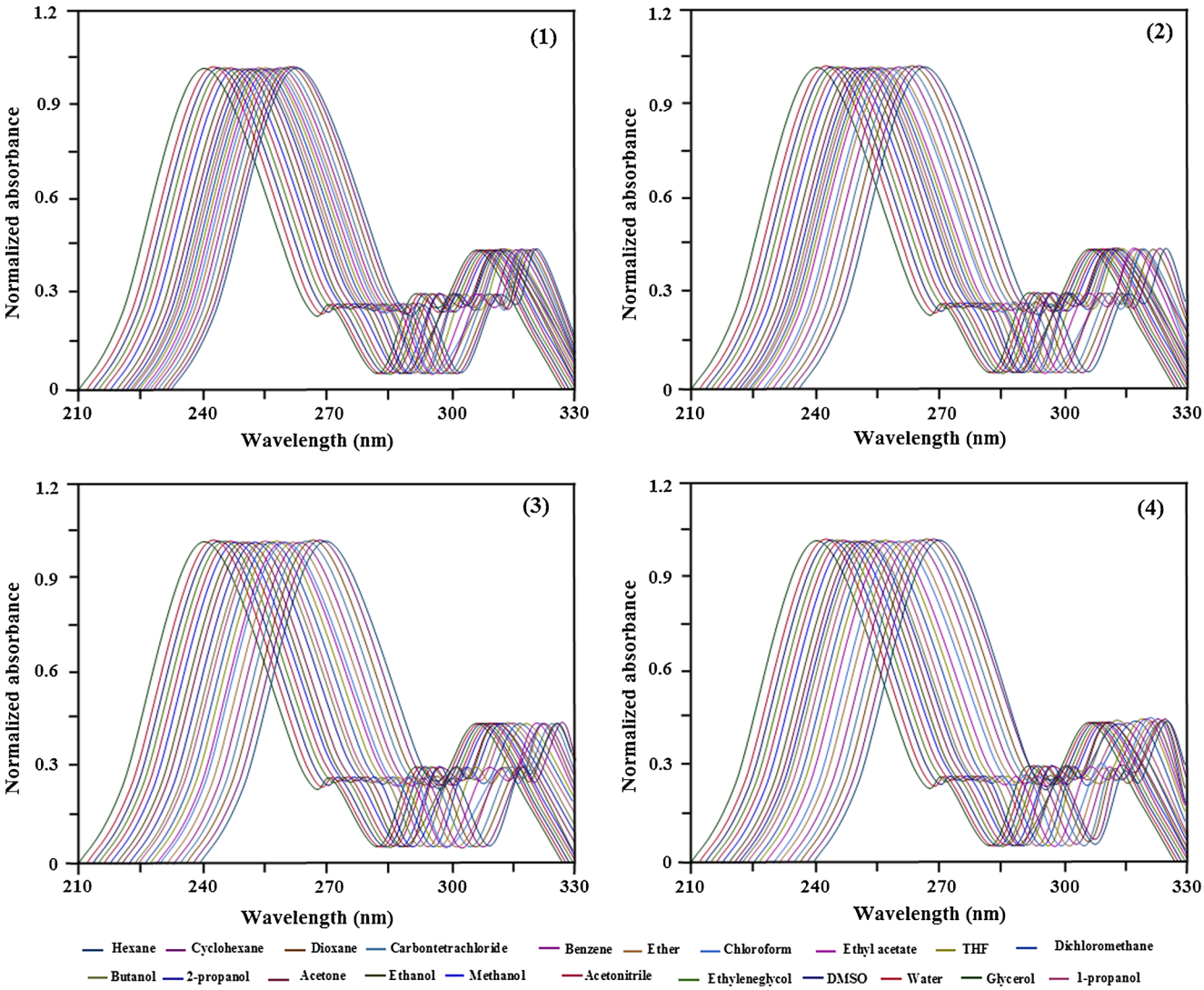

Fig. 1 Absorption spectra of 1-4 in different solvents

the polarity of the medium and intramolecular charge transfer (CT) state.

In order to obtain an insight about specific solvent—fluorophore interactions, the influence on fluorescence emission of 1 in methanol–water mixtures of different composition has been monitored and the spectra are illustrated in Fig. 3b. The addition of water to methanol–water mixture remarkably enhances the fluorescence of 1 with red shift. This effect may be described by the combined effect of hydrogen bonding and polarity of the medium. Mixing of two closely lying lowest singlet states (n, π*and π, π*) of phenanthroimidazole derivatives favours the intersystem crossing [18]. As the polarity of the medium is increased, intermolecular hydrogen bonding interaction in the excited state stabilized the π, π* state and enhancing the energy between the two states, which diminishes the mixing between the states (Scheme 2). As a result intersystem crossing from S_1 to T_1 decreases and an enhancement of fluorescence is observed. The same trend has been observed for compound 2–4.

The behaviour of phenanthroimidazole derivatives toward different solvent polarities may be interpreted in terms of the difference in the ground state and the excited state dipole moments. The spectral shift in fluorescence band may be attributed to the interaction between the dipole moment of the solute and the polarizability of the solvent. The extent of charge separation on electronic excitation of 1–4 have been determined by measuring the change in the dipole moment ($\Delta\mu=\mu_e-\mu_g$) utilizing the spectral shift between the absorption and emission maxima as a function of solvent polarity. According to Lippert–Mataga equation [19].

$$\bar{\nu}_{ss} = \bar{\nu}_{ab} - \bar{\nu}_{fl} = const + \left[\frac{2\left(\mu_e - \mu_g\right)^2}{hca^3}\right] f(D,n) \qquad (4)$$

where $f(D,n)=(D-1)/(2D+1)-(n^2-1)/(2n^2+1)$, which indicates the orientation polarizability and depicts polarity

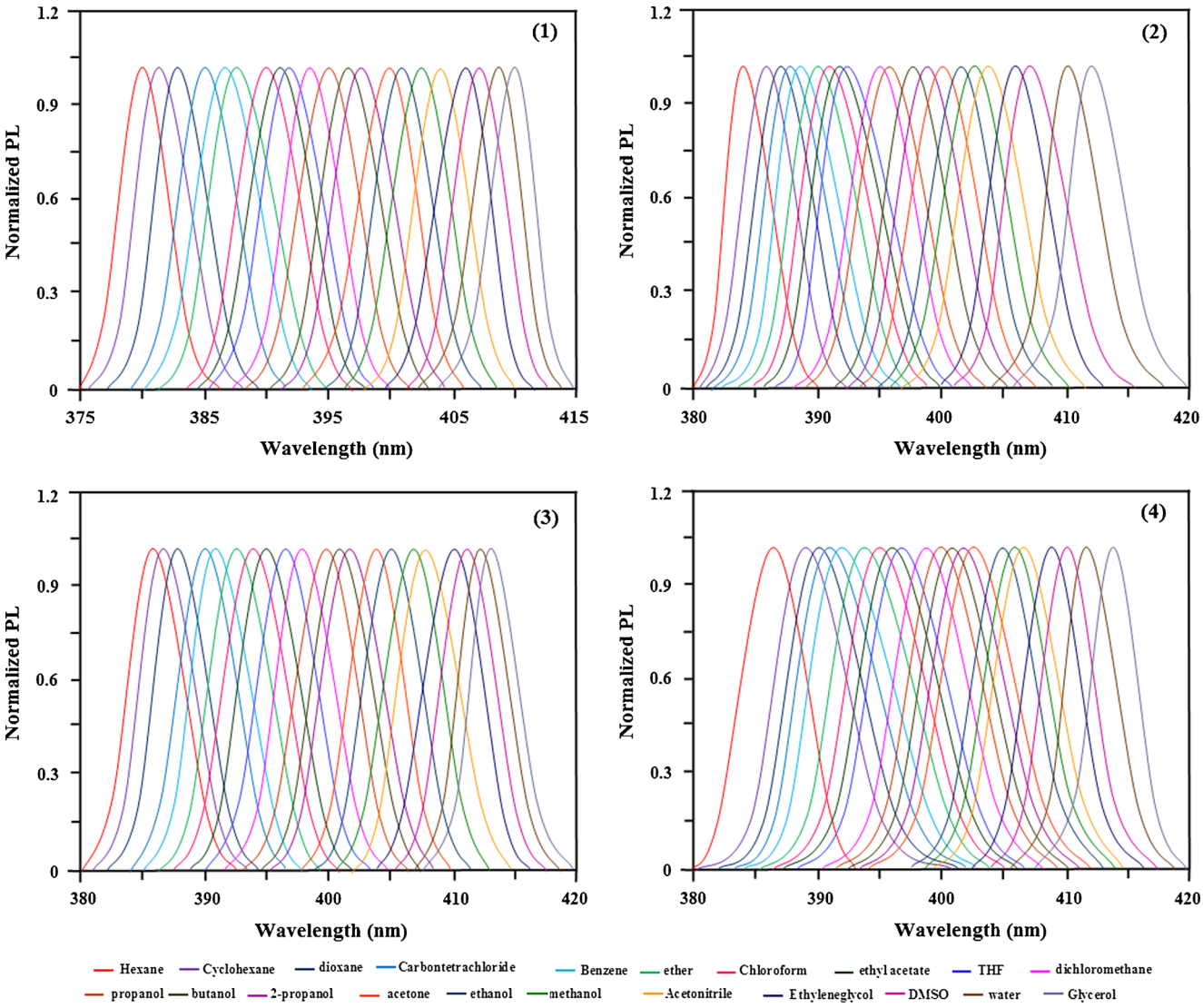

Fig. 2 Emission spectra of 1-4 in different solvents

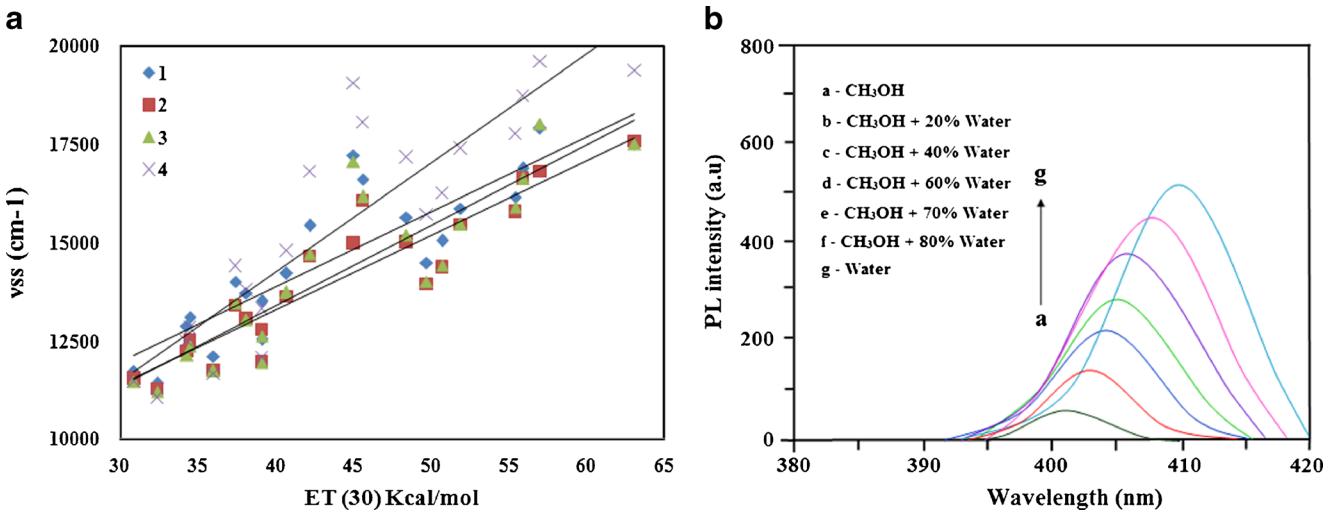

Fig. 3 **a** Stokes shift with E_T (30); **b** Methanol- water diagram of 1

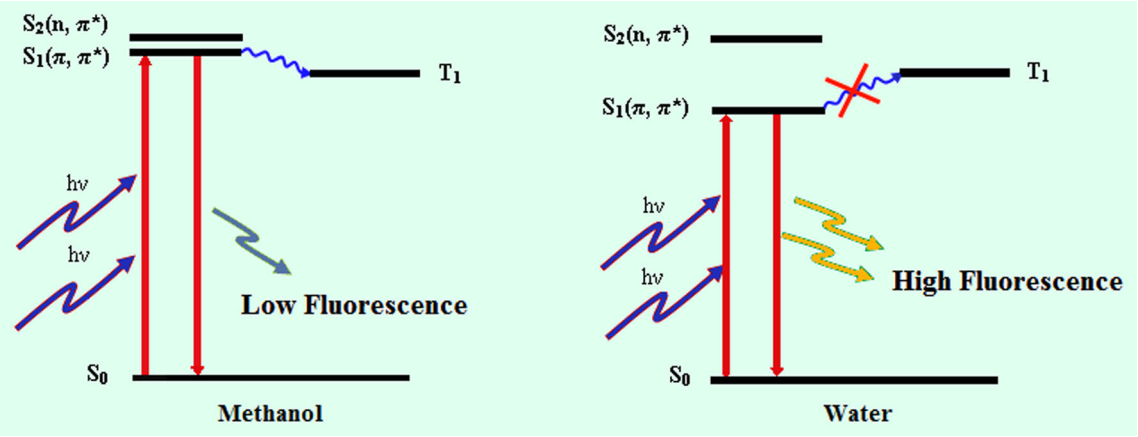

Scheme 2 Intersystem crossing from S1 to T1 state

parameter of the solvent, n is refractive index, D is dielectric constant, μ_e and μ_g are dipole moments of the species in S_1 and S_0 states, respectively, h is Planck's constant, c is velocity of light and a is Onsager's cavity radius. The Lippert-Mataga plot is linear for the non-polar and polar/aprotic solvents as shown in Fig. 4a; correlation is satisfactory. The geometrical optimization of 1–4 was done by DFT method using Gaussian-03 [20] to calculate the μ_g. Using μ_g value, 5.56D (1), 5.72D (2), 5.83D (3) and 5.75D (4) obtained from the DFT calculation and the slope of Lippert–Mataga plot, the value of μ_e calculated is in the range, 14.0–.23.0 D for the studied phenanthriimidazoles.

Multiple linear regression analysis is performed to identify the different modes of solvation determining the absorption and emission energies. Kamlet and Taft [21] put forward the π^*, α and β parameters to characterize the polarity/polarizability, the acidity and the basicity of a solvent respectively. Conversely, Catalan et al. [22] proposed an empirical solvent scales for polarity/polarizability (SPP), acidity (SA) and basicity (SB) to describe the respective properties of a given solvent

$$y_{=}y_0 + a_\alpha\alpha + b_\beta\beta + c_{\pi*}\pi^* \quad \text{(Kamlet}--\text{Taft)} \tag{5}$$

$$y_{=}y_0 + a_{SA}SA + b_{SB}SB + c_{SPP}SPP \quad \text{(Catalan)} \tag{6}$$

The dominant coefficient affecting the absorption and fluorescence band of phenanthroimidazole derivatives (1–4) are displayed in Table 2. Negative values of solvent dipolar interaction (π^*) and hydrogen bond accepting property (β) indicate these two parameters contribute to the stabilization of both the ground and the excited states of phenanthroimidazole derivatives. The calculated ratio of α over π^* [1.31(υ_{abs}) & 1.49 (υ_{emi}) (1), 2.19(υ_{abs}) & 2.75(υ_{emi}) (2), 1.89(υ_{abs}) & 2.08(υ_{emi}) (3) and 2.77 (υ_{abs}) & 4.06(υ_{emi}) (4)] reveal that interactions between phenanthroimidazole derivatives and solvents with acidity property (α) predominate in the excited state. A good linear variation is also obtained between the fluorescence maxima

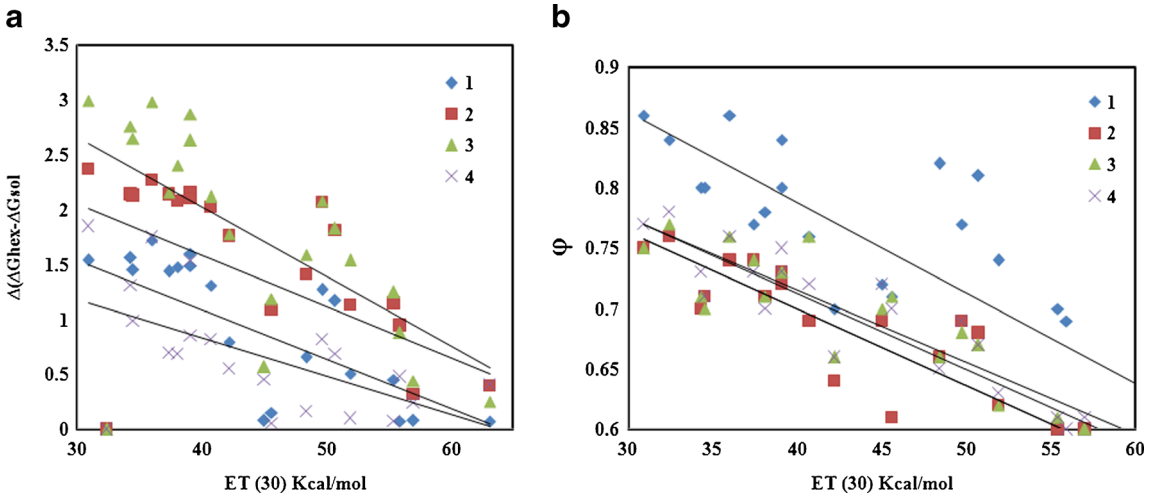

Fig. 4 **a** Lippert – Mataga diagram; **b** Fluorescence maxima and E_T (30) values

Table 2 Adjusted coefficients ($(\upsilon_x)_0$, c_a, c_b and c_c) for the multilinear regression Analysis of the Absorption υ_{abs} and fluorescence υ_{emi} wavenumbers and stokes shift ($\Delta\upsilon_{ss}$) of 1–4 with the solvent polarity/polarizability, and the acid and base capacity using the Taft (π*, α and β) and the Catalan (SPP^N, SA and SB) scales

cmpd.	(υ_x)	$(\upsilon_x)_0 cm^{-1}$	(π*)	c_α	c_β
1	λ_{abs}	$(2.728\pm0.015)\times10^4$	$-(3.386\pm2.639)\times10^3$	$(7.998\pm8.496)\times10^3$	$-(4.542\pm6.654)\times10^3$
	λ_{emi}	$(3.816\pm0.024)\times10^4$	$(1.848\pm4.357)\times10^3$	$-(6.896\pm14.025)\times10^3$	$(6.187\pm10.983)\times10^3$
	$\Delta\upsilon_{ss}=\upsilon_{abs}-\upsilon_{emi}$	$(1.088\pm0.092)\times10^4$	$(5.242\pm3.245)\times10^3$	$-(14.914\pm10.445)\times10^3$	$(10.742\pm8.180)\times10^3$
	(υ_x)	$(\upsilon_x)_0 cm^{-1}$	c_{SPP}^N	c_{SA}	c_{SB}
	λ_{abs}	$(3.761\pm0.060)\times10^4$	$(7.641\pm6.791)\times10^3$	$-(21.620\pm17.990)\times10^3$	$-(17.131\pm13.474)\times10^3$
	λ_{emi}	$(2.763\pm0.040)\times10^4$	$-(4.510\pm4.545)\times10^3$	$(8.536\pm12.040)\times10^3$	$-(3.907\pm9.018)\times10^3$
	$\Delta\upsilon_{ss}=\upsilon_{abs}-\upsilon_{emi}$	$(0.099\pm0.038)\times10^4$	$(12.166\pm4.375)\times10^3$	$-(30.191\pm11.590)\times10^3$	$(21.063\pm8.681)\times10^3$
2	(υ_x)	$(\upsilon_x)_0 cm^{-1}$	(π*)	c_α	c_β
	λ_{abs}	$(3.774\pm0.017)\times10^4$	$(1.982\pm4.026)\times10^3$	$-(2.611\pm13.448)\times10^3$	$(0.898\pm10.701)\times10^3$
	λ_{emi}	$(2.598\pm0.008)\times10^4$	$(0.219\pm1.888)\times10^3$	$(0.202\pm2.306)\times10^3$	$-(0.349\pm5.018)\times10^3$
	$\Delta\upsilon_{ss}=\upsilon_{abs}-\upsilon_{emi}$	$(1.175\pm0.014)\times10^4$	$(1.762\pm3.217)\times10^3$	$-(2.812\pm10.747)\times10^3$	$(1.247\pm8.552)\times10^3$
	(υ_x)	$(\upsilon_x)_0 cm^{-1}$	c_{SPP}^N	c_{SA}	c_{SB}
	λ_{abs}	$(3.792\pm0.015)\times10^4$	$-(1.415\pm6.070)\times10^3$	$(10.316\pm26.878)\times10^3$	$-(10.084\pm29.334)\times10^3$
	λ_{emi}	$(2.607\pm0.006)\times10^4$	$-(3.752\pm2.498)\times10^3$	$(19.101\pm11.061)\times10^3$	$-(20.627\pm12.071)\times10^3$
	$\Delta\upsilon_{ss}=\upsilon_{abs}-\upsilon_{emi}$	$(1.185\pm0.012)\times10^4$	$(2.337\pm4.841)\times10^3$	$(8.693\pm21.438)\times10^3$	$(10.544\pm23.396)\times10^3$
3	(υ_x)	$(\upsilon_x)_0 cm^{-1}$	(π*)	c_α	c_β
	λ_{abs}	$(3.72\pm0.034)\times10^4$	$(5.54\pm6.201)\times10^3$	$-(9.84\pm19.958)\times10^3$	$(2.75\pm15.630)\times10^3$
	λ_{emi}	$(2.52\pm0.047)\times10^4$	$-(3.74\pm8.591)\times10^3$	$(3.48\pm37.653)\times10^3$	$(0.72\pm21.656)\times10^3$
	$\Delta\upsilon_{ss}=\upsilon_{abs}-\upsilon_{emi}$	$(1.20\pm0.069)\times10^4$	$(9.26\pm12.542)\times10^3$	$-(13.29\pm40.369)\times10^3$	$(1.83\pm31.615)\times10^3$
	(υ_x)	$(\upsilon_x)_0 cm^{-1}$	c_{SPP}^N	c_{SA}	c_{SB}
	λ_{abs}	$(3.68\pm0.011)\times10^4$	$(4.18\pm11.392)\times10^3$	$-(3.02\pm30.179)\times10^3$	$-(4.34\pm22.604)\times10^3$
	λ_{emi}	$(2.62\pm0.012)\times10^4$	$-(12.13\pm13.084)\times10^3$	$(20.77\pm34.661)\times10^3$	$-(9.10\pm25.961)\times10^3$
	$\Delta\upsilon_{ss}=\upsilon_{abs}-\upsilon_{emi}$	$(1.06\pm0.018)\times10^4$	$(16.29\pm20.446)\times10^3$	$-(23.76\pm54.163)\times10^3$	$(4.74\pm40.568)\times10^3$
4	(υ_x)	$(\upsilon_x)_0 cm^{-1}$	(π*)	c_α	c_β
	λ_{abs}	$(3.74\pm0.014)\times10^4$	$(2.63\pm2.472)\times10^3$	$-(4.77\pm7.957)\times10^3$	$(2.35\pm6.232)\times10^3$
	λ_{emi}	$(2.23\pm0.042)\times10^4$	$-(6.58\pm7.739)\times10^3$	$(19.3\pm24.908)\times10^3$	$-(13.31\pm19.507)\times10^3$
	$\Delta\upsilon_{ss}=\upsilon_{abs}-\upsilon_{emi}$	$(1.51\pm0.032)\times10^4$	$(9.22\pm5.914)\times10^3$	$-(24.06\pm19.036)\times10^3$	$(15.65\pm14.908)\times10^3$
	(υ_x)	$(\upsilon_x)_0 cm^{-1}$	c_{SPP}^N	c_{SA}	c_{SB}
	λ_{abs}	$(3.73\pm0.037)\times10^4$	$(1.54\pm4.235)\times10^3$	$-(91.75\pm11.220)\times10^3$ $(40.86\pm32.685)\times10^3$	$-(1.99\pm8.404)\times10^3$
	λ_{emi}	$(2.34\pm0.109)\times10^4$	$-(15.67\pm12.338)\times10^3$	$-(40.74\pm26.066)\times10^3$	$-(28.81\pm24.481)\times10^3$
	$\Delta\upsilon_{ss}=\upsilon_{abs}-\upsilon_{emi}$	$(1.38\pm0.087)\times10^4$	$(17.21\pm9.839)\times10^3$		$(26.79\pm19.523)\times10^3$

and E_T (30) values [23] as shown by Fig. 4b. The free energy change of solvation and reorganization energies of 1–4 in various solvents have been estimated (Table 3). According to Marcus [24], $E(A)=\Delta G_{solv}+\lambda_1$ and $E(F)=\Delta G_{solv}-\lambda_0$, where E(A) and E(F) are absorption and fluorescence band maxima in cm^{-1}, respectively, ΔG_{solv} is the difference in free energy of the ground and excited states in a given solvent and λ represents the reorganization energy . The free energy change of solvation and reorganization energies of 1–4 in various solvents has been estimated. Under the condition that $\lambda_0\approx\lambda_1\approx\lambda$, we get, $E(A)+E(F)=2\Delta G_{solv}$; $E(A)-E(F)=2\lambda$. The ΔG_{solv} of 1–4 is maximum for hexane since it is purely non-polar and also α and β values of hexane are zero. The ΔG_{solv} is minimum in water. The difference between these values (water and hexane) should give the free energy change required for hydrogen bond formation. The plot of $\Delta(\Delta G_{solv})=(\Delta G_{hex}-\Delta G_{water})$ versus $E_T(30)$ has been depicted in Fig. 5a. The difference in free energy of solvation in hexane and different hydrogen bonding solvents (i.e. ΔG_{solv}) of 1–4 follow the order of the hydrogen bond energy [25]. In the aprotic solvents the values are small and interaction of phenanthroimidazole derivatives with those solvents is purely due to dipolar interactions in the excited state. The reorganization energy values of 1–4 have also been determined in different solvents. The definite values of reorganization energy confirmed the interaction between low frequency motions such as reorientation of solvent cell with low and medium frequency nuclear motion of the solute.

Fluorescence Lifetime and Quantum Yield

The time correlated single photon counting (TCSPC) results fit to single exponentials decay

$$f(t) = \alpha_1 \exp\ (-t/\tau_1) \quad (7)$$

Table 3 Absorption maxima (λabs max, nm), fluorescence emission maxima (λab max, nm), Stokes shift (ν_{ss}, cm^{-1}), fluorescence quantum yield ($\overline{\Phi}_f$), life time (τ, ns), radiative rate constant (k_r, s^{-1}), nonradiative rate constant (k_{nr}, s^{-1}) and log(k_r/k_{nr}) of 4 in various solvents

Solvents	$\overline{\nu}_{ss}$	ΔG (kcal/mol)	$\Delta(\Delta G_{hex}-\Delta G_{sol})$	λ (kcal/mol)	Φ	τ	k_r	K_{nr}	$\log(k_r/k_{nr})$ (10^8)
Hexane	4877.89	91.34	0.00	15.80	0.78	1.3	0.6	0.16	5.5
Cyclohexane	4850.092	89.49	1.85	16.38	0.77	1.3	0.59	0.17	5.2
Dioxane	4795.205	89.59	1.75	16.67	0.76	1.3	0.58	0.18	5.0
Carbon tetrachloride	4835.053	89.81	1.53	17.25	0.75	1.3	0.57	0.19	4.8
Benzene	5264.584	90.03	1.31	17.84	0.73	1.3	0.56	0.20	4.3
Ether	5332.48	90.35	0.99	18.34	0.71	1.4	0.50	0.20	3.9
Chloroform	4474.109	90.49	0.85	19.03	0.73	1.4	0.52	0.19	4.3
Ethyl acetate	4694.971	90.65	0.69	19.72	0.7	1.4	0.5	0.21	3.7
THF	4789.888	90.64	0.70	20.58	0.73	1.4	0.52	0.19	4.3
Dichloromethane	5116.057	90.52	0.82	21.14	0.72	1.4	0.51	0.2	4.1
Propanol	6174.461	91.53	0.82	22.46	0.69	1.4	0.49	0.22	3.5
Butanol	6396.919	90.65	0.69	23.23	0.67	1.6	0.42	0.20	3.1
2-propanol	5621.021	91.79	0.55	24.01	0.66	1.6	0.41	0.21	2.9
Acetone	6069.699	90.18	0.16	24.55	0.65	1.5	0.43	0.23	2.7
Ethanol	5906.309	91.24	0.10	24.86	0.63	1.6	0.39	0.23	2.3
Methanol	6513.597	91.27	0.07	25.40	0.61	1.6	0.38	0.24	1.9
Acetonitrile	5745.556	91.29	0.05	25.79	0.7	1.6	0.43	0.18	3.7
Ethylene glycol	6366.135	90.86	0.48	26.77	0.6	1.6	0.37	0.25	1.8
DMSO	6037.91	90.89	0.45	27.23	0.72	1.5	0.48	0.18	4.1
Water	5420.585	90.93	0.41	27.68	0.58	1.4	0.41	0.3	1.4

where α_1 and τ_1 are respectively, the pre-exponential factor and lifetime of the various excited states involved. DAS6 software was used for the fit and the χ^2 values are always less than 1.2. The fluorescence lifetime measurements of all phenanthroimidazole derivatives were made in ethanol with laser excitation set at 270 nm and the fluorescence signal was measured at the emission wavelength of individual compound. The absolute PL quantum yields were measured by comparing fluorescence intensities (integrated areas) of a standard sample (Coumarin 46) and the unknown sample using the formula

$$\Phi_{unk} = \Phi_{std}\left(\frac{I_{unk}}{I_{std}}\right)\left(\frac{A_{std}}{A_{unk}}\right)\left(\frac{\eta_{unk}}{\eta_{std}}\right)^2 \quad (8)$$

where, Φ_{unk} is the fluorescence quantum yield of the sample, Φ_{std} is the fluorescence quantum yield of the standard; I_{unk} and I_{std} are the integrated emission intensities of the sample

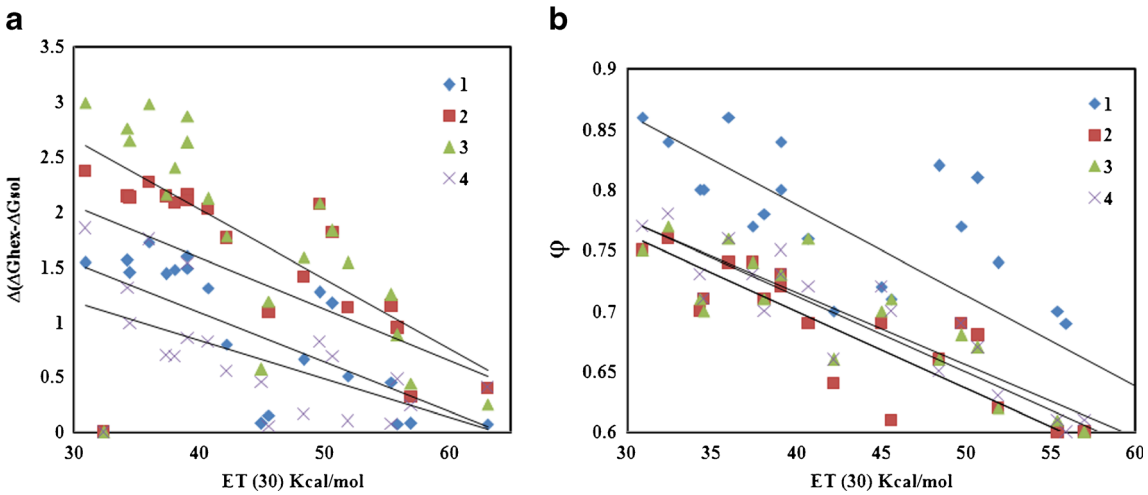

Fig. 5 **a** Δ (ΔG_{solv}) versus $E_T(30)$; **b** φ_f with solvent polarity parameter E_T (30)

and the standard, respectively. A_{unk}, and A_{std} are the absorbances of the sample and the standard at the excitation wavelength, respectively. η_{unk} and η_{std} are the indexes of refraction of the sample and standard solutions. Fluorescence quantum yield (φ_f) was measured in solvents of different polarity and presented in Table 3. The radiative and non-radiative decay of the excited state of 1–4 have been obtained using the quantum yields and lifetimes. The formula employed to calculate the radiative (k_r) and non-radiative (k_{nr}) rate constants is $k_r=\Phi_p/\tau$; $k_{nr}=(1/\tau)-(\Phi_p/\tau)$; $\tau=(k_r+k_{nr})^{-1}$, where k_r and k_{nr} are the radiative and non-radiative deactivation, τ_f is the lifetime of the S_1 excited state. A typical set of k_r and k_{nr} values are tabulated (Table 3). Perusal of the radiative and non-radiative rate constants shows that in most of the cases the radiative emission is predominant over non-radiative transitions.

The variation of φ_f with solvent polarity parameter E_T (30) is depicted in Fig. 5b. The result shows that the φ_f values in various solvents are sensitive towards solvent polarity. The remarkable increase of φ_f in polar protic medium is compared with that in polar aprotic medium. This may be due to differential contribution of CT and hydrogen bonding interactions. Radiative (k_r) and nonradiative (k_{nr}) rate constants are calculated from fluorescence quantum yields and lifetime values (Fig. 6a) in different solvents to understand the effect of solvation on the dynamics of the excited state. The logarithm of (k_r/k_{nr}) is plotted against the solvent polarity parameter E_T (30) which is shown in Fig. 6b. Two different straight lines are obtained, one for aprotic solvents and the other for protic solvents. In both the cases, upon increasing the polarity the logarithm ratio of radiative to nonradiative rate decreases but a steeper slope is obtained in the case of protic solvents. It indicates that the radiative and nonradiative rates are more sensitive toward protic solvents. It may be that the hydrogen bonding interaction in polar protic environment enhances the stabilization of the S_1 state as a result the nonradiative relaxation rate increases [26].

An interesting result is provided by the blue shift of the CT absorption bands with increasing solvent polarity (Fig. 7a) [13, 27]. With the assumption that point dipole is at the center of the spherical cavity and the mean solute polarizability (α) to be insignificant, it follows,

$$hc\tilde{\upsilon}_{abs}\approx hc\tilde{\upsilon}_{abs}^{vac}-2\mu_g\left(\mu_e-\mu_g\right)/\alpha_o^3[(\varepsilon-1/2\ \ \varepsilon+1)-{}^1/_2(n^2-1/2n^2+1)] \quad (9)$$

where μ_g and μ_e are the dipole moments of the solute in the ground and excited state, correspondingly, ν_{abs} and $\tilde{\upsilon}_{abs}^{vac}$ are the spectral positions of a solvent-equilibrated absorption maxima and the value extrapolated to the gas-phase, respectively, a_o is the effective radius of the Onsager cavity, [28] and ε and n are the static dielectric constant and the refractive index of the solvent, respectively. In the case of the well-separated CT absorption bands, Eq. 9 is used to determine the values of $\mu_g(\mu_e-\mu_g)/\alpha_o{}^3$ and $\tilde{\upsilon}_{abs}^{vac}$. In the excited state, the negative and positive ends of the electric dipole are localized nearly in the centres of the donor and acceptor fragments respectively. A considerable red shift of their spectral position and the increase of the Stokes shift and enlargement of the emission bandwidth with increasing solvent polarity in fluorescence spectra point to the CT character of the fluorescent states and clearly indicate that the absolute values of μ_e are much higher than those of μ_g. The excited state dipole moments μ_e can be estimated by the fluorescence solvatochromic shift method due to the fact that the excited states live sufficiently long with respect to the orientation relaxation time of the solvent [29–31]. Under the same assumptions as used for expression 4, it follows that

$$hc\tilde{\upsilon}_{flu}\approx hc\tilde{\upsilon}_{flu}^{vac}-2\mu_e\left(\mu_e-\mu_g\right)/\alpha_o^3[(\varepsilon-1/2\ \ \varepsilon+1)\ \ -{}^1/_2(n^2-1/2n^2+1)] \quad (10)$$

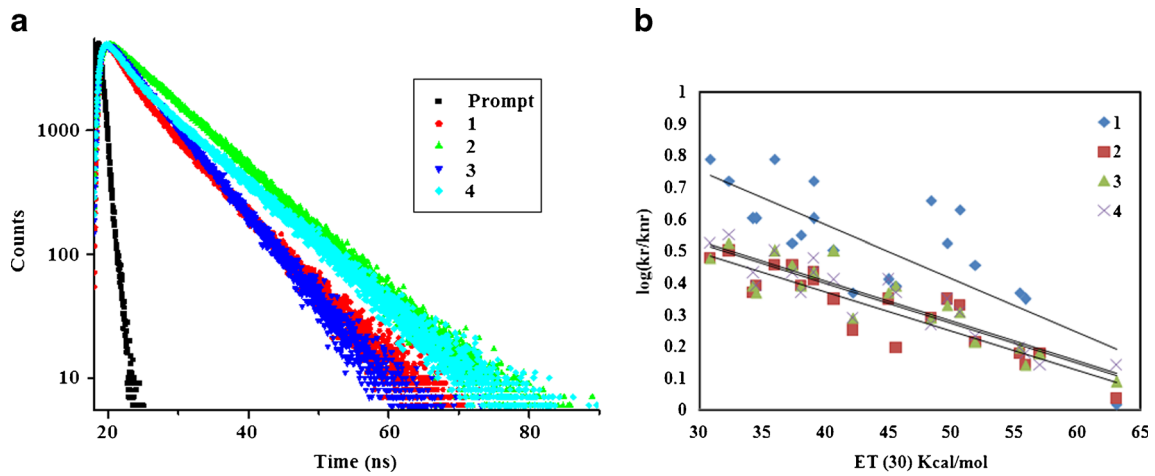

Fig. 6 **a** Lifetime spectra of 1-4; **b** log (k_r/k_{nr}) Vs $E_T(30)$

where $\tilde{\upsilon}_{flu}$ and $\tilde{\upsilon}_{flu}^{vac}$ are the spectral positions of the solvent equilibrated fluorescence maxima and the value extrapolated to the gas-phase, respectively. The compounds studied show a satisfying linear correlation between the energy $hc\tilde{\upsilon}_{flu}$ and the solvent polarity function in a polar environment and also in all the solvents (Fig. 7b) [32]. The values of $\mu_e(\mu_e-\mu_g)/\alpha_o{}^3$ extracted from the data measured in polar media are somewhat larger than those resulting from the analysis of the data obtained for the whole range of the solvents. This finding can be explained only by the dependence of the electronic structure of the fluorescent states on solvation. Due to a relatively small energy gap between the lowest internal charge transfer (ICT) states and the states excited locally in the nonpolar solvents, which leads to increase of the contribution of the (π, π *) character to the wave function of the CT states. It leads to a lowering of energy with respect to a pure CT state because of a stabilizing character of such interactions and red shift obtained in the fluorescence spectra.

Under the assumption that the CT fluorescence corresponds to the state reached directly upon excitation, the quantity $(\mu_e-\mu_g)^2/\alpha_o{}^3$ can be evaluated from the solvation effects on the Stokes shift,

$$hc\left(\tilde{\upsilon}_{abs}-\tilde{\upsilon}_{flu}\right)=hc\left(hc\tilde{\upsilon}_{abs}^{vac}-hc\tilde{\upsilon}_{flu}^{vac}\right)+2\left(\mu_e-\mu_g\right)^2/\alpha_o^3\left[(\varepsilon-1/2\ \ \varepsilon+1)\ \ {}^{-1}/_{2}\ \ \left(n^2-1/2n^2+1\right)\right] \tag{11}$$

The compounds studied show a satisfying linear correlation between the energy $hc\tilde{\upsilon}_{abs}-hc\tilde{\upsilon}_{flu}$ and the solvent polarity function in a polar environment and also in all the solvents studied; the values of $(\mu_e-\mu_g)/\alpha_o{}^3$ are 0.62 eV (1), 0.66 eV (2), 0.72 eV (3) and 1.23 eV (4). The equations 9–11 relate the measured quantities to the excited state dipole moments μ_e. Under the assumption that $\mu_e>>\mu_g$ and with the effective spherical radius of the molecules a_0, 5.94 Aº (1), 5.91 Aº (2), 5.98 Aº (3) and 5.99 Aº (4), as estimated from the molecular dimensions of the compounds calculated by molecular mechanics, equations 10 and 11 yield very similar values of μ_e being in the range of 14.40 D (1), 13.29 D (2), 18.68 D (3) and 22.52 D (4) for the studied molecules. The large value of $\Delta\mu=\mu_e-\mu_g\approx$8.06 D (1), 9.64 D (2), 13.99 D (3) ad 17.7 D (4) corresponds to a charge separation of about 0.3 nm, 0.4 nm, 0.5 nm and 0.4 nm which roughly agrees with the centre-to-centre distance between the donor and acceptor moieties of the compound.

This conclusion is in agreement with a linear relationship found between the CT fluorescence energies and the differences in the redox potentials corresponding to the oxidation of the donor subunit E_{oxi} (D) and the reduction of the acceptor moiety E_{red} (A) in the D-A molecules. The correlation is shown in Fig. 8. In this correlation the values of E_{oxi} (D)$-E_{red}$ (A) are taken from the electrochemical data obtained for the given D-A molecule in ACN containing 0.1 M $TBAPF_6$. These values are very similar to those expected from the electrochemical properties of the donor and acceptor alone. The small shift of E_{red} (A) to more negative potentials can be explained by the electron donating properties of substituted phenanthroimidazole fragment bonded to the acceptor subunit. Correspondingly, the small shift of E_{oxi} (D) to more positive potentials arises from the electron withdrawing character of the acceptor moiety. The E_{red} (A) and E_{oxi} (D) values indicate also (in agreement with the absorption spectra) that both subunits of all the D-A molecules studied interact very weakly.

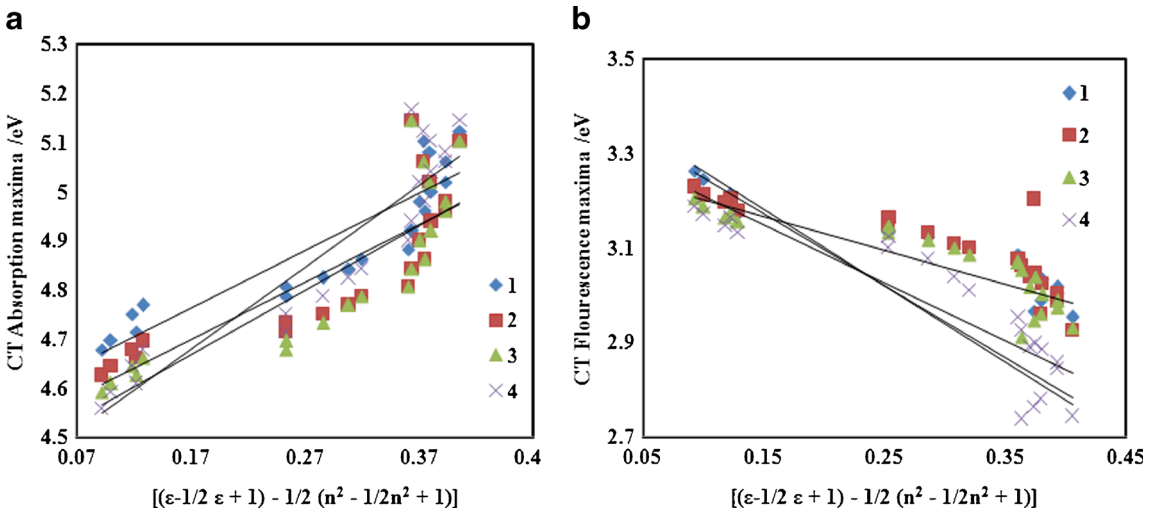

Fig. 7 **a** CT Absorption maxima Vs solvent polarity function; **b** CT Fluorescence maxima Vs solvent polarity function

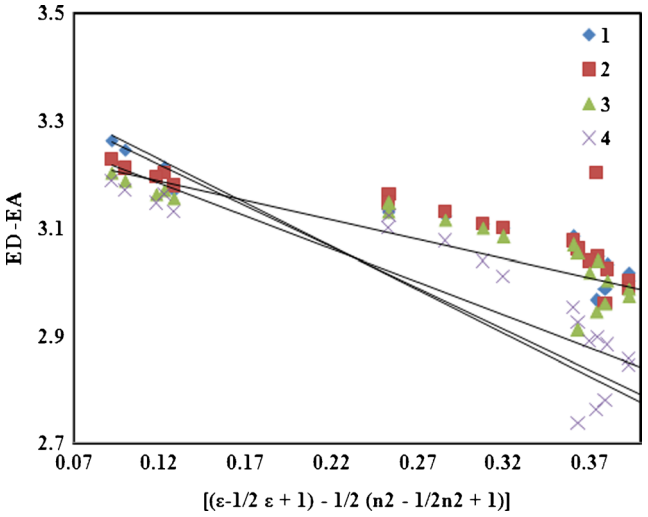

Fig. 8 ED-EA Vs SPF

This finding points to a different electronic structure of the emitting singlet state CT of 1–4. The spectroscopic CT state can be regarded as a linear combination of the zero-order ET state (^{1}ET) with: (i) various locally excited $^1(\pi, \pi^*)$ states and (ii) with the ground state, S_0 [33] :

$$\psi^1_{CT} \cong C_{ET}\phi^1_{ET} + C_a\phi^1_a + C_b\phi^1_b + C_0\phi^1_0 \quad (12)$$

where $\phi_0{}^1, \phi_{ET}{}^1, \phi_a{}^1$ and $\phi_b{}^1$ represent the closed-shell configuration of the ground state, the zero-order wave functions of the pure ^{1}ET state (which is described by a full ET from the occupied orbital HOMO of the donor to the vacant LUMO orbital of the acceptor) and the $L_a{}^1$ and $L_b{}^1$ states of the donor moieties, respectively. The values of Δμ suggest that the wave functions $\psi_{CT}{}^1$ of the ^{1}CT states are in the order 4>3>2 >1. This finding is in agreement with the value of $hc\tilde{\upsilon}^{vac}_{abs}$ mixing of the lowest pure ^{1}ET state with the $^1(\pi, \pi^*)$ excitations leads to the lowering of the spectroscopic ^{1}CT state energy due to a stabilising character of such interactions. It is also in agreement with the magnitude of the electronic coupling elements $V_1{}^D$ estimated from Eq. 12; one can expect that the contribution of the $^1(\pi, \pi^*)$ character to the wave function $\psi_{CT}{}^1$ should decrease in the order: 4>3>2 >1.

Electronic Coupling Elements

The electronic coupling elements between the lowest excited ^{1}CT state and the ground state (V_0) or the locally excited state lying most closely in energy (V_1) can be estimated from the CT absorption and fluorescence investigations. Applying a simple kinetic model of an irreversible excited CT state Formation (with 100 % efficiency), the radiative and non-radiative rate constants, k_r and k_{nr}, and the resulting electronic transition dipole moments M_{flu} are given by [34, 35]:

$$k_f = \frac{64\pi 4}{3h}\left(n\tilde{\upsilon}^{vCT}_{flu}\right)^3 |M_{flu}| \quad (13)$$

The electronic transition dipole moments M_{flu} can be expressed by the following relation [1, 2, 7]

$$M_{flu} = C_{ET}\ V_0\left(\mu_e - \mu_g\right)/hc\tilde{\upsilon}^{vCT}_{flu} + \sum{}_i CiMi \quad (14)$$

The first term in the above equation corresponds the Mulliken two-state model [4, 5] (i.e., the interactions between the solvent equilibrated fluorescent CT state and the Franck–Condon ground state), the second one represents the Murrell 'borrowing' mechanism [6] (i.e., the contributions from the locally excited states i of energy E_i) . The electronic transition dipole moments M_i correspond radiative transitions (^{1}LE)$_i \rightarrow$ S_0 (states i in the studied systems to the ^1L_a and ^1L_b states of the donor moieties, cf. Eq. 12).

The fluorescence analysis of the studied compounds do not allow us to determine the electronic coupling elements between the fluorescent CT state and the ground state (V_0) or the locally excited states ($V_1{}^D$) . The situation seems to be considerably simplified for 1–4 because of the relatively small contribution of the locally excited (π, π*) configurations to the wave function $\psi_{CT}{}^1$ of the fluorescent state (Eqs. 3 and 12). For these compounds in highly polar media, similarly as for carbazol-9-yl derivatives of aromatic nitriles [1] and aryl derivatives of aromatic amines [2], due to the large energy gap between the ^{1}CT fluorescent state and ^{1}LE states as well as the lowering of the transition energy $hc\tilde{\upsilon}^{CT}_{flu}$, the M_{flu} values can be approximated assuming the dominant electronic coupling between the fluorescent state and the ground state. Neglecting the second term in Eq. 14 and assuming that the c_{ET} value is close to unity, the V_0, 0.18 eV (1), 0.11 eV(2), 0.19 eV(3) and 0.12 eV(4) value calculated with $\Delta\mu = \mu_e - \mu_g \approx 8.06$D (1), 9.64 D(2), 13.99 D(3) and 17.7 D(4). This quantity is very close to the values calculated from Eq. 1.

The reorganisation energy λ_0 is related to the low-frequency motions such as reorientation of the solvent shell λ_s as well as any other low-frequency and medium frequency nuclear motions of the solute ($\delta\lambda_0$). The inner reorganization energy λ_i corresponds to the high-frequency motions associated with the changes in the solute bond lengths and angles. The values of the low-frequency reorganization energy λ_0 depend on the solvent polarity Fig. 9a, as expected. Within the continuum dielectric model of solvation, an analysis of the solvatochromic effects on λ_0 is possible according to the following expression [1, 2] :

$$\lambda_0 \approx \delta\lambda_0 + \lambda_0 \approx \delta\lambda_0 + \left(\mu_e - \mu_g\right)^2/\alpha_o^3\left[(\varepsilon - 1/2\ \varepsilon + 1) - {}^1/_2\ (n^2 - 1/2n^2 + 1)\right] \quad (15)$$

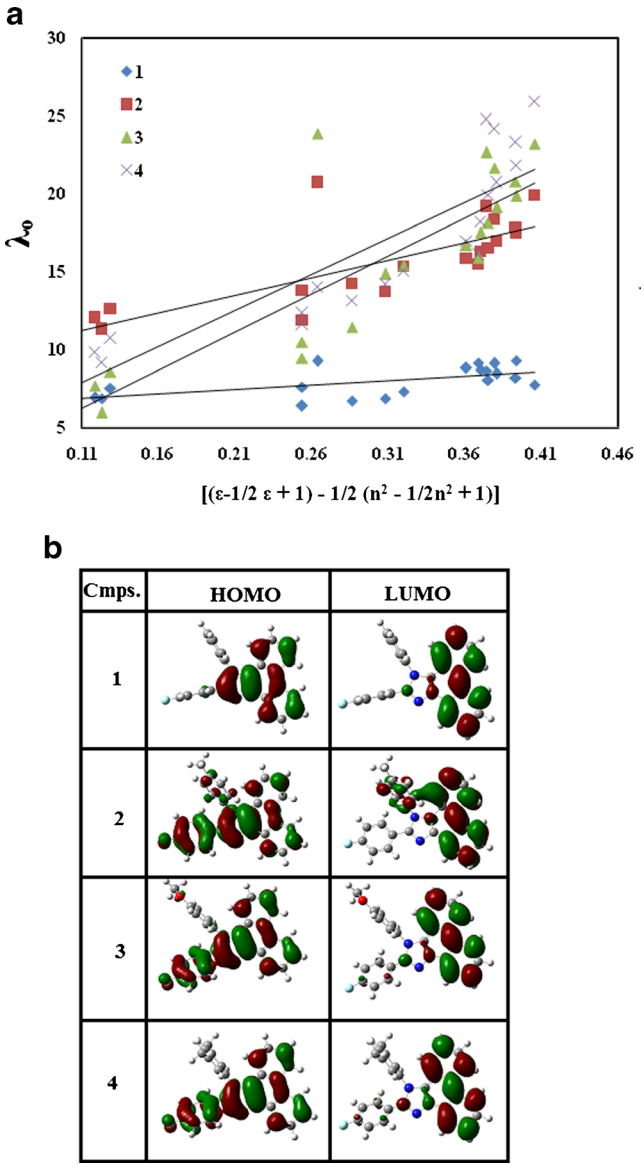

Fig. 9 **a** λo depend on the solvent polarity function; **b** HOMO-LUMO maps of 1-4

This relation is suitable for the direct comparison with the results of the investigations of the solvatochromic effects on the spectral position of the CT fluorescence maxima (Fig. 7b). The values of $(\mu_e-\mu_g)^2/\alpha_o{}^3$ (0.58 eV (1), 0.65 eV (2), 0.74 eV (3) and 1.20 eV (4) obtained from the mean slope of the plots corresponding to Eq.15 agree with those collected in Table 4. This finding supports again the hypothesis that the wave functions $\psi_{CT}{}^1$ of the ^{1}CT states of the order 4>3>2>1.

The electrochemical properties of the phenanthroimidazole derivatives (1–4) have been examined by cyclic voltammetry and the redox potentials have been measured from the plot potential versus current. The energies of the highest occupied molecular orbital (HOMO) and lowest unoccupied molecular orbital (LUMO) have been calculated using the relation, $E_{HOMO} = 4.8 + E_{1/2}{}^{oxi}$; $E_{LUMO} = E_{HOMO}-1239/\lambda_{onset}$ and the calculated values are given in Table 4. The 3D plot of HOMO−LUMO orbital picture is shown in (Fig. 9b). The LUMO energies have been deduced from the HOMO energies and the lowest-energy absorption edges of the UV–vis absorption spectra. The calculated energy gap ($E_g=E_{HOMO}-E_{LUMO}$) of 1–4 are 2.82, 3.94, 2.68 and 3.05 eV. Therefore, the HOMO stability and the emission energy gap are controlled by the nature and substituent present in the phenanthroimidazole moiety.

Conclusions

Solvent-induced transformation of the electronic structure of the ^{1}CT states of selected D–A phenanthroimidazole derivatives containing fluorine as an electron acceptor has been analysed in terms of a model combining the Mulliken–Murrell theory of the CT complexes and the Marcus theory of the radiative charge recombination $^1CT \rightarrow S_0$. Analysis of the electronic coupling elements show that the differences in the photophysical properties of the studied molecules can be interpreted in terms of the different electronic interactions between the CT state and the ground state (V_0) and/or the $^1(\pi, \pi^*)$ excited states most probably localized in the donor moiety $V_1{}^D$. This approach can be used to explain the solvatochromic effects on the spectral position of the CT fluorescence spectra as well as on the M_{flu} values. The conformation of the investigated D–A systems in the fluorescent CT states seems to be the similar to that in the ground state.

Table 4 Slopes and intercepts of the solvatochromic plots of the CT Fluorescence of the imidazoles (1–4)

compound	μg_D	$\mu_e(\mu_e-\mu_g)/\alpha_o{}^3$	$hc\tilde{\upsilon}_{abs}^{vac}$, eV	θ	D_{HOMO}	D_{LUMO}	V_0	V_1D
1	4.40	0.75	3.76	0.75	1.32	14.67	1.11	0.08
2	3.65	0.66	4.02	0.66	1.30	16.23	2.21	0.18
3	4.69	0.72	4.25	0.72	1.10	25.77	2.50	0.12
4	4.82	1.78	4.81	1.78	2.01	16.99	2.95	0.10

Acknowledgments One of the authors Prof. J. Jayabharathi is thankful to DST [No. SR/S1/IC-73/2010], DRDO (NRB-213/MAT/10-11) and CSIR (NO 3732/NS-EMRII) for providing funds to this research study.

References

1. Kapturkiewicz A, Herbich J, Karpiuk J, Nowacki J (1997) Intramolecular radiative and radiadtionless charge recombinations in donor-acceptor carbazole derivatives. J Phys Chem A 101:2332
2. Herbich J, Kapturkiewicz A (1998) Electronic structure and molecular conformation in the excited charge transfer singlet states of p-acridyl and other aryl derivatives of aromatic amines. J Am Chem Soc 120:1014
3. Herbich J, Kapturkiewicz A, Nowacki J (1996) Phosphorescent intramolecular charge-transfer states. Chem Phys Lett 262:633
4. Mulliken RS (1952) J Am Chem Soc 74:811
5. Mulliken RS, Person WB (1969) Molecular complexes: a lecture and reprint volume. Wiley, New York
6. Murrell JN (1959) J Am Chem Soc 81:5037
7. Bixon M, Jortner J, Verhoeven J (1994) Lifetimes for radiative charge recombination in donor-acceptor molecules. J Am Chem Soc 116:7349–7355
8. Gould IR, Young RH, Mueller LJ, Albrecht AC, Farid S (1994) J Am Chem Soc 116:8188
9. Dogonadze RR, Kuznetsov AM, Marsagishvili TA (1980) The present state of the theory of charge transfer in condensed phase. Electro Chim Acta 25:1–28
10. Mataga N, Kaifu Y, Koizumi M (1955) Bull Chem Soc Jpn 28:690
11. Bigelow RW, Johnson GE (1977) J Phys Chem 66:4861
12. Gudipati MS, Daverkausen J, Maus M, Hohlneicher G (1994) Higher electrnically excited states of phenanthrene, carbazole and fluorine. Chem Phys 186:289–301
13. Chiba K, Aihara J-I, Araya K, Matsunaga Y (1980) Bull Chem Soc Jpn 53:1703
14. Pramanik S, Banerjee P, Sarkar A, Mukherjee A, Mahalanabis KK, Bhattacharya SC (2008) Spectroscopic investigation of 3-Pyrazolyl 2-Pyrazoline derivative in homogeneous solvents. Spectrochim Acta Part A 71:1327–1332
15. Willard DM, Riter RE, Levinger NE (1998) J Am Chem Soc 120:4151
16. Saha S, Samanta A (2002) J Phys Chem A 106:4763
17. Reichardt C (1988) Solvents and solvent effects in organic chemistry, 2nd edn. VCH, Weinheim
18. de Melo JSS, Becker RS, Macanita AL (1994) J Phys Chem 98:6054
19. Lippert E (1957) Spektroskopische bistimmung des dipolmomentes aromatischer verbindugen imersten angeregten singulettzustand. Z Electrochem 61:962–975
20. Frisch MJ, Trucks GW, Schlegel HB, Scuseria GE, Robb MA, Cheeseman JR, Montgomery JA, Vreven T Jr, Kudin KN, Burant JC, Millam JM, Iyengar SS, Tomasi J, Barone V, Mennucci B, Cossi M, Scalmani G, Rega N, Petersson GA, Nakatsuji H, Hada M, Ehara M, Toyota K, Fukuda R, Hasegawa J, Ishida M, Nakajima T, Honda Y, Kitao O, Nakai H, Klene M, Li X, Knox JE, Hratchian P, Cross JB, Adamo C, Jaramillo J, Gomperts R, Stratmann RE, Yazyev O, Austin AJ, Cammi R, Pomelli C, Ochterski JW, Ayala PY, Morokuma K, Voth GA, Salvador P, Dannenberg JJ, Zakrzewski VG, Dapprich S, Daniels AD, Strain MC, Farkas O, Malick DK, Rabuck AD, Raghavachari K, Foresman JB, Ortiz JV, Cui Q, Baboul AG, Clifford S, Cioslowski J, Stefanov BB, Liu G, Liashenko A, Piskorz P, Komaromi I, Martin RL, Fox DJ, Keith T, Al-Laham MA, Peng CY, Nanayakkara A, Challacombe M, Gill PMW, Johnson B, Chen W, Wong MW, Gonzalez C, Pople JA (2004) Gaussian 03, Revision C.02. Gaussian, Inc., Wallingford
21. Kamlet MJ, Taft RW (1976) J Am Chem Soc 98:377–383
22. Catalan J, Lopez V, Perez P (1996) Use of the SPP scale for the analysis of molecular system with dual emissions resulting from the solvent polarity. J Fluoresc 6:15–22
23. Reichardt C (1979) Empirical parameters of solvent polarity as linear free energy relationships. Angew Chem Int Ed Engl 18:98–110
24. Marcus RA (1963) J Chem Phys 38:1858
25. Castellan GW (1985) Physical Chemistry, 3rd edn. Narosa Publishing House, Delhi
26. Dhar S, Rana DK, Roy SS, Roy S, Bhattacharya S, Bhattacharya SC (2012) Effect of solvent environment on the photophysics of a newly synthesized bioactive 7-oxy(5-selenocyanato-pentyl)-2H-1-benzopyran- 2-one. J Lumin 132:957–964
27. Rettig W, Zander M (1982) On Twisted Intramolecular Charge Transfer (TICT) stated in N-aryl-carbazoles. Chem Phys Lett 87:229–234
28. Onsager LJ (1936) J Am Chem Soc 58:1486
29. Böttcher CJF (1973) In: Van Belle OC, Bordewijk P, Rip A (eds) In theory of electric polarization. Elsevier, Amsterdam, Vol. I
30. Lippert EZ (1955) Naturforsch A10:541
31. Liptay W (1974) In: Lim EC (ed) In Excited States. Academic, New York, p 129
32. McRae EG (1957) Theory of solvent effects on molecular electronic spectra, frequency shifts. J Phys Chem 61:562–572
33. Mulliken RS, Person WB (1969) Molecular complexes: a ture and reprint volume. Wiley, New York
34. Birks JB (1970) Photophysics of aromatic molecules. Wiley, New York, p 51
35. Michl J, Thulstrup EW (1986) Spectroscopy with Polarized Light. VCH, New York, pp 28–75